NOTES AND CORRESPONDENCE

Influence of Albedo Variability in Complex Terrain on Mesoscale Systems

R. A. PIELKE, J. H. RODRIGUEZ, J. L. EASTMAN, R. L. WALKO, AND R. A. STOCKER

Department of Atmospheric Science, Colorado State University, Fort Collins, Colorado

1 October 1992 and 2 March 1993

1. Introduction

Recently, a series of studies has demonstrated the influence of spatial variations of transpiring vegetation on the structure of the planetary boundary layer and development of mesoscale systems (e.g., Segal et al. 1988; Segal et al. 1989; Pielke and Zeng 1989; Avissar and Pielke 1989; André et al. 1989; Chang and Wetzel 1991). The need to represent this spatial variation in vegetation in larger-scale models, such as general circulation models (GCMs), has been demonstrated in those papers.

Any surface heterogeneity, however, that results in spatial variations in sensible heat flux can generate mesoscale circulations, as reported in Pielke et al. (1991). This short contribution illustrates observed variations in albedo as measured from a geostationary satellite in which most of the variability is due to different geological formations. While slope and aspect of the terrain have some influence on the albedo since the direct insolation of the sun intercepts the surface at different angles [e.g., see Eqs. (11)–(29) in Pielke 1984], most of the variation results from the type of soil and rock surface.

Previous investigations of albedo variations include those of Otterman (1977) and Mahrer and Pielke (1978). In those works, the denudation of the Sinai peninsula of dry plant material by uncontrolled grazing goats, as contrasted with the controlled grazing in the Negev Desert, resulted in substantial albedo differences. The Sinai was cooled by as much as 9°C.

2. Methodology

Due to the large variation in the albedo of a given surface, an appropriate procedure to calculate the surface albedo is to have measurements on the order of a few meters and then to average the values over larger spatial areas that are still much smaller than the Rossby radius (Dalu et al. 1991). This latter constraint is required because horizontal variations in surface heating can cause coherent mesoscale fluxes to develop that are a substantial fraction of or larger than the chaotic turbulent fluxes over the same area when the heat patches are a substantial fraction of the Rossby radius. For larger spatial scales ($\approx$100–500 km), however, the database would be unmanageable. However, visible satellite measurements can produce albedo values with a footprint on the order of 1 km, so that the influence of albedo variations on spatial scales of several kilometers and larger can be determined.

Surface albedos can be calculated from satellite brightness counts by first converting the brightness counts to radiative fluxes by using a bidirectional reflectance model and then converting these narrowband radiant fluxes to broadband radiant fluxes. The surface albedos calculated in the following section followed an algorithm developed by Minnis and Harrison (1984).

a. Test cases

In order to illustrate the seasonal variation of albedo on a large mesobeta-scaled domain, we chose a region with complex terrain and selected a summer and a winter test case.

Figure 1 shows the topography of the selected area, A_1, which is located in northern Arizona. This area was used to perform the model simulations because computer limitations would not permit a larger domain. The albedo statistics are calculated for this domain, as well as for larger domain A. The geographic area of the study is shown in Fig. 2.

The summer case chosen to analyze and model was 7 June 1986 and for the winter case, 10 February 1986. Both days were clear of large amounts of clouds, a condition necessary in order to calculate surface albedos. Figures 3 and 4 show the visible satellite images for the June and February cases, respectively. Extensive snow cover is evident for the winter case, while only the highest elevations have snow on the chosen June date.

Corresponding author address: Dr. Roger A. Pielke, Department of Atmospheric Science, Colorado State University, Fort Collins, CO 80523.

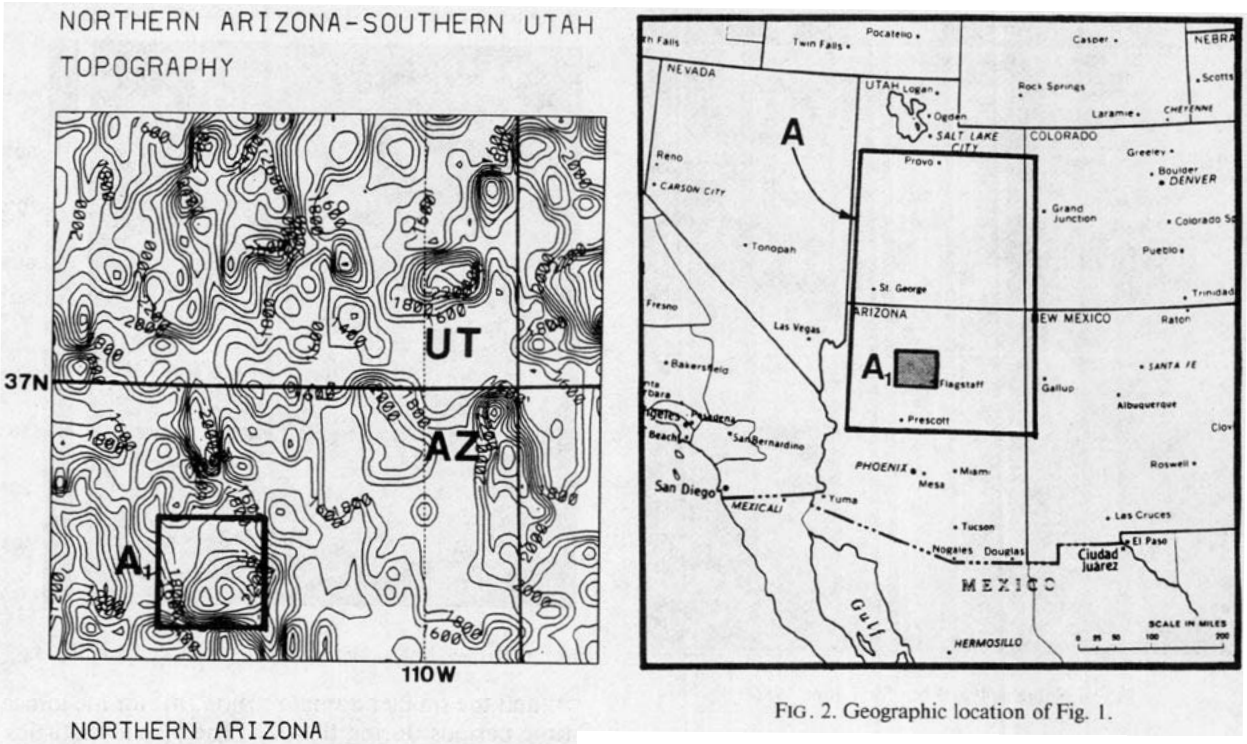

FIG. 2. Geographic location of Fig. 1.

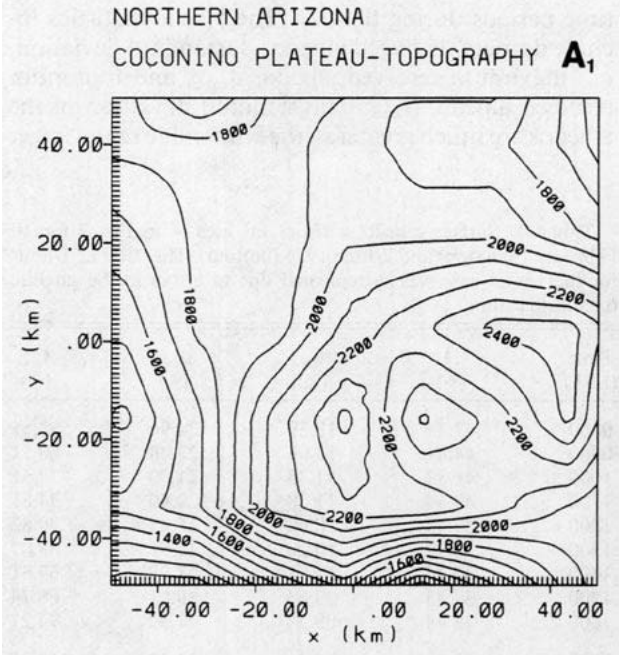

FIG. 1. Terrain contours in the northern Arizona–southern Utah area (top) and for the region labeled A_1 (bottom). Contour interval is 100 m.

b. *Albedo results*

Figures 5 and 6 represent the albedo contour maps at 1100 LST for the summer and winter cases over area A. In order to plot this albedo data, the raw albedo values were processed through a two-dimensional smoother to eliminate large discontinuities between grid points. Therefore, by using a filter, the larger-scale trends were retained and the mean albedos of the two

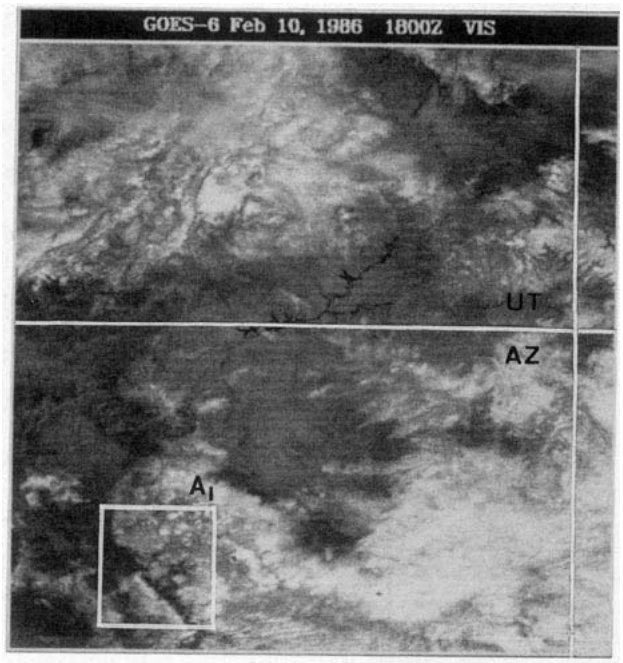

FIG. 3. GOES satellite image for 10 February 1986 at 1100 LST for the region shown in Fig. 1.

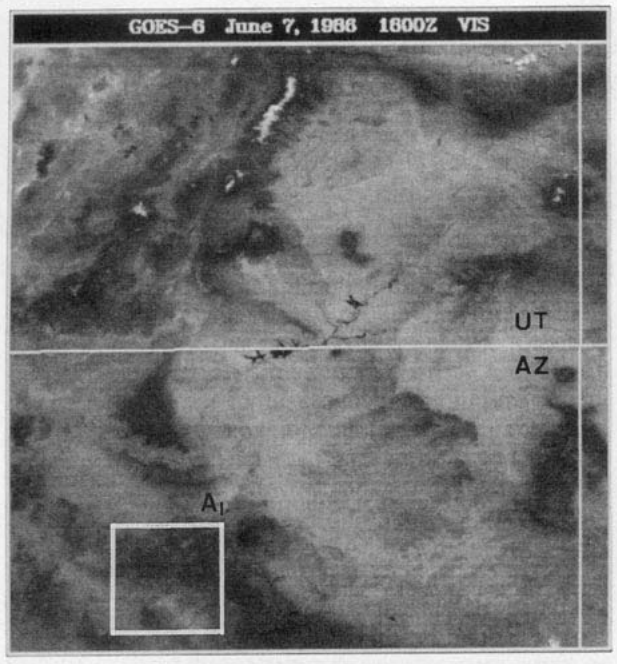

FIG. 4. Same as Fig. 3 but for 7 June 1986.

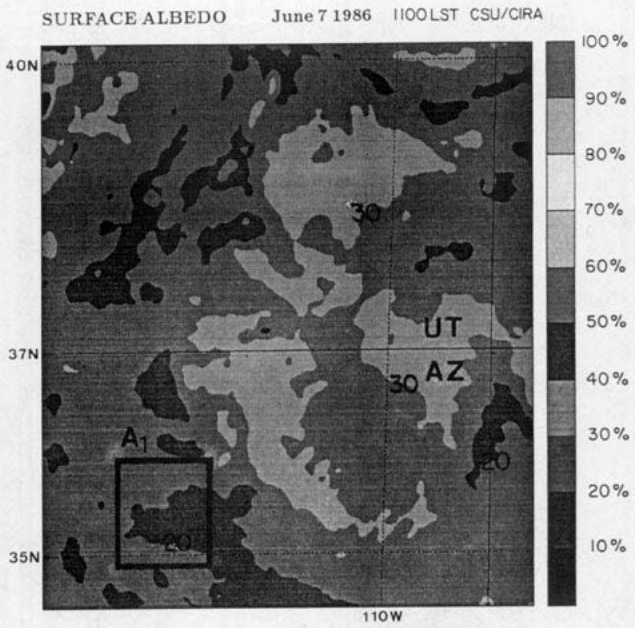

FIG. 6. Surface albedo for the satellite image shown in Fig. 4.

cases were not changed although the maximum and minimum values were shifted toward the mean.

Tables 1 and 2 show several calculated statistics for the nonfiltered albedo data over the entire study area, A, and the smaller domain region, A_1, for the indicated time periods during the day. The albedo statistics include domain-averaged albedo, $\bar{A}$, standard deviation, σ_A, maximum resolved albedo, A_{max}, and minimum resolved albedo, A_{min}. The standard deviation of the albedos are much greater in the winter due to the larger

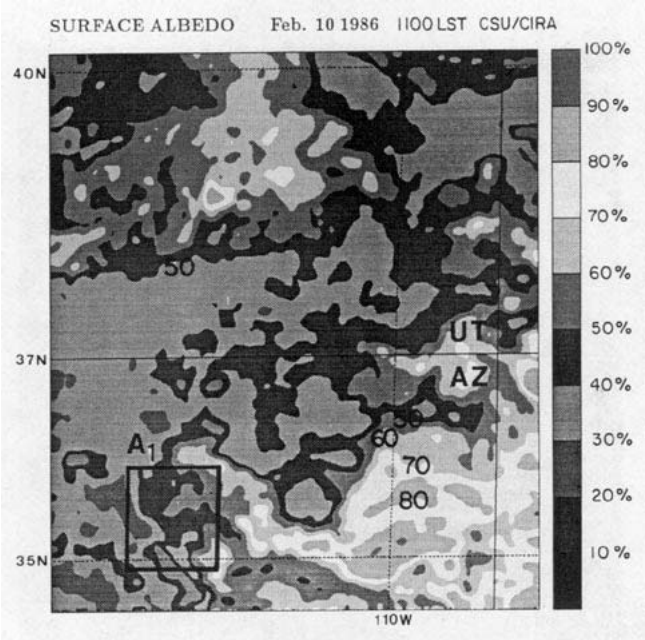

FIG. 5. Surface albedo for the satellite image shown in Fig. 3. Contour interval is 10% and is labeled in several places to make the gray shading clearer.

TABLE 1. Surface albedo statistics for area A in Fig. 2 for 10 February 1986 (top) and 7 June 1986 (bottom). The 0800 LST hour for the winter case was extrapolated due to errors in the satellite data at that time.

Time (LST)	$\bar{A}$ (%)	σ_A (%)	A_{min} (%)	A_{max} (%)
0800	47.75	12.39	24.96	82.51
0900	44.81	12.06	22.48	80.51
1000	41.87	11.73	21.00	78.51
1100	40.54	11.30	20.40	74.61
1200	39.38	10.68	18.45	70.82
1300	38.39	10.20	19.91	68.07
1400	37.62	10.05	18.97	67.81
1500	37.43	09.63	19.01	66.74
1600	38.94	09.54	21.32	74.27
0800	33.68	6.41	21.32	62.25
0900	28.07	5.34	17.77	51.88
1000	30.28	5.63	19.04	56.74
1100	25.70	4.58	15.90	48.93
1200	21.12	3.65	13.09	37.61
1300	20.94	3.83	12.84	55.13
1400	29.36	5.79	17.95	78.09
1500	28.82	5.99	17.78	93.03
1600	26.15	6.69	16.54	90.04

TABLE 2. Same as Table 1 but for area A_1.

Time (LST)	$\bar{A}$ (%)	σ_A (%)	A_{min} (%)	A_{max} (%)
0800	49.06	13.88	19.10	80.07
0900	47.55	13.42	19.64	79.61
1000	46.04	12.96	21.36	79.15
1100	44.62	13.09	21.02	78.27
1200	42.65	13.09	20.78	78.87
1300	41.71	13.80	19.17	81.29
1400	39.57	12.88	18.38	71.66
1500	41.14	12.71	19.49	72.84
1600	42.71	12.53	19.66	73.36
0800	31.65	4.68	18.58	48.36
0900	28.48	4.66	17.92	42.24
1000	27.34	4.23	17.16	38.56
1100	26.19	3.82	16.86	36.06
1200	21.40	2.94	14.05	29.39
1300	21.17	3.00	13.60	29.26
1400	24.82	3.69	16.11	35.42
1500	28.47	4.55	18.26	41.82
1600	32.12	5.19	20.09	49.88

differences in soil moisture during the winter and the presence of large areas of new snow. The mean winter albedo is also about twice as large as in the summer. Examination of the raw data also implies that the albedo is normally distributed around the mean.

c. *Model results*

The modeling work reported in this section was completed using the Regional Atmospheric Modeling System (RAMS, see Pielke et al. 1992 for a recent description of this modeling tool). The Regional Atmospheric Modeling System was set up with the model

TABLE 3. Model characteristics used in RAMS.

Parameter	Characteristic
Δx, Δy	1 km
Δt	10 s
Horizontal domain	100 × 100 km^2
Vertical levels	25
Atmosphere	nonhydrostatic, horizontally homogeneous
Lateral boundary conditions	Klemp and Wilhelmson (1978a,b)
Upper boundary conditions	wall on top
Albedo	$A(t)$ and $A(x, y, t)$
Soil type	sandy clay loam
Soil model	Tremback and Kessler (1985)
Soil moisture	summer 10% saturated, winter 5% saturated
Radiation type	Mahrer and Pielke (1977)
Synoptic wind	0 m s^{-1}
Initial time	1500 UTC (0800LST)
Run time	9 hours

TABLE 4. Simulations performed using RAMS.

Run	Case	Topography type	Albedo	Code
1	winter	complex	$A(t)$	TOPO $A(t)$
2	winter	flat	$A(t)$	NOTOPO $A(t)$
3	summer	complex	$A(t)$	TOPO $A(t)$
4	summer	flat	$A(t)$	NOTOPO $A(t)$
5	winter	complex	$A(x, y, t)$	TOPO $A(x, y, t)$
6	winter	flat	$A(x, y, t)$	NOTOPO $A(x, y, t)$
7	summer	complex	$A(x, y, t)$	TOPO $A(x, y, t)$
8	summer	flat	$A(x, y, t)$	NOTOPO $A(x, y, t)$

parameters indicated in Table 3. The simulation domain is A_1. It was not feasible to model the entire area A with our existing computer resources; however, the computation of the albedo statistics (see Tables 1 and 2) showed that area A_1 is representative of the larger-scale area. A series of experiments, as summarized in Table 4, were performed to evaluate the relative importance of albedo variations contrasted with terrain variations over the area. The model was integrated for a daylight period for the winter and summer case study days. Zero large-scale flow was assumed.

Figures 7 and 8 present the horizontal wind field 28 m above the ground. These figures demonstrate that the simulation with flat terrain and observed albedo spatial variations results in mesoscale flows that are apparently as substantial (i.e., horizontal winds of 5 to 10 m s^{-1}) as the mesoscale flow that develops in the actual complex terrain but with a uniform albedo [TOPO $\bar{A}(t)$].

These results are more quantitatively compared in Figs. 9 and 10 where the mesoscale fluxes are averaged at several heights above local ground level across the model domain and contrasted with the subgrid-scale (i.e., turbulent) fluxes over the same area. The mesoscale fluxes are calculated from

$$\langle w'\theta' \rangle_D = \langle (w - \langle w \rangle_D)(\theta - \langle \theta \rangle_D) \rangle_D,$$

where $\langle \ \rangle_D$ refers to a domain average at a given height, while the turbulent fluxes are obtained from:

$$\langle \overline{w''_Z \theta''_Z} \rangle_D = - \frac{\langle \overline{w''_s \theta''_s} \rangle_D [(\alpha + 1)Z - \langle Z_i \rangle_D]}{\langle Z_i \rangle_D}, \quad (1)$$

where $\langle \overline{w''_Z \theta''_Z} \rangle_D$ is the turbulent heat flux at some level $Z (0 \leq Z \leq Z_i)$, $\langle Z_i \rangle_D$ is the domain-averaged height of the boundary layer, $\alpha = 0.2$, and $\langle \overline{w''_s \theta''_s} \rangle_D$ is the subgrid-scale heat flux at the surface, with $\langle \overline{w''_s \theta''_s} \rangle_D = - \langle u_* \theta_* \rangle_D$, where u_* is the *friction velocity* and θ_* is called the *flux temperature*. By linear interpolation, using Eq. (1), the domain-averaged subgrid-scale vertical heat fluxes at any height within the boundary layer can be calculated. While the winter fluxes are substan-

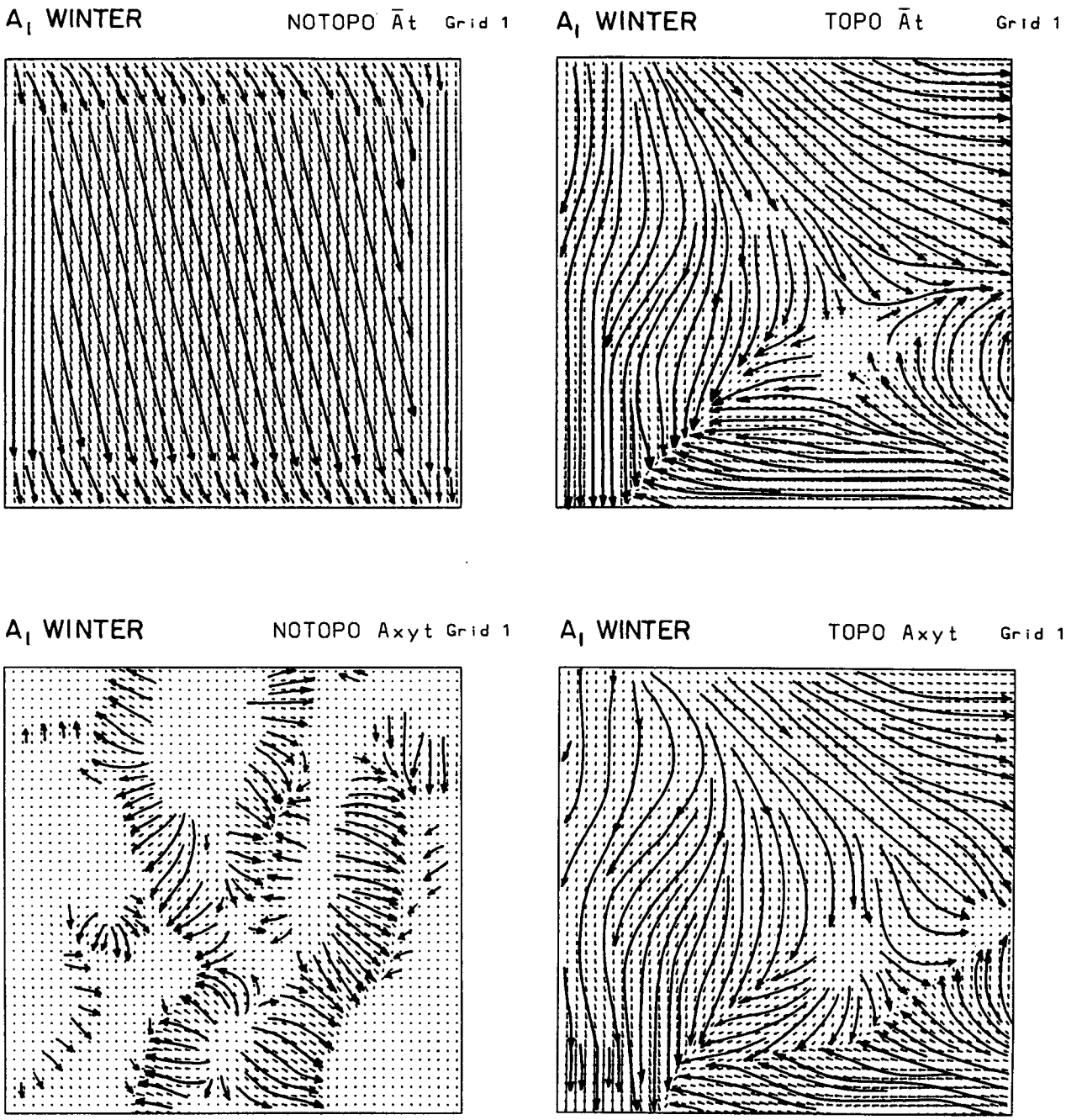

FIG. 7. RAMS simulated horizontal wind field at 28.3 m at 1300 LST for the four winter sensitivity simulations listed in Table 4. The wind direction for each case is illustrated using streamlines that are superimposed on the wind vectors at each grid point. These streamlines define direction only and do not indicate speed. Note that mesoscale flow develops a steady flow in the flat, constant in space simulation (top left) because RAMS randomly perturbs momentum fluxes when the wind is near zero. These random momentum fluxes directly feed into the heat fluxes. Horizontal gradients of surface heat flux eventually result in the development of significant mesoscale flows, as also shown in Fig. 10.

tially less because the solar insolation is weaker, the mesoscale fluxes are still important as contrasted with the subgrid-scale fluxes, particularly well above the surface. At hour 7, for example, the mesoscale heat fluxes for the cases of terrain and albedo variations, and albedo variations alone at 346 m are on the order

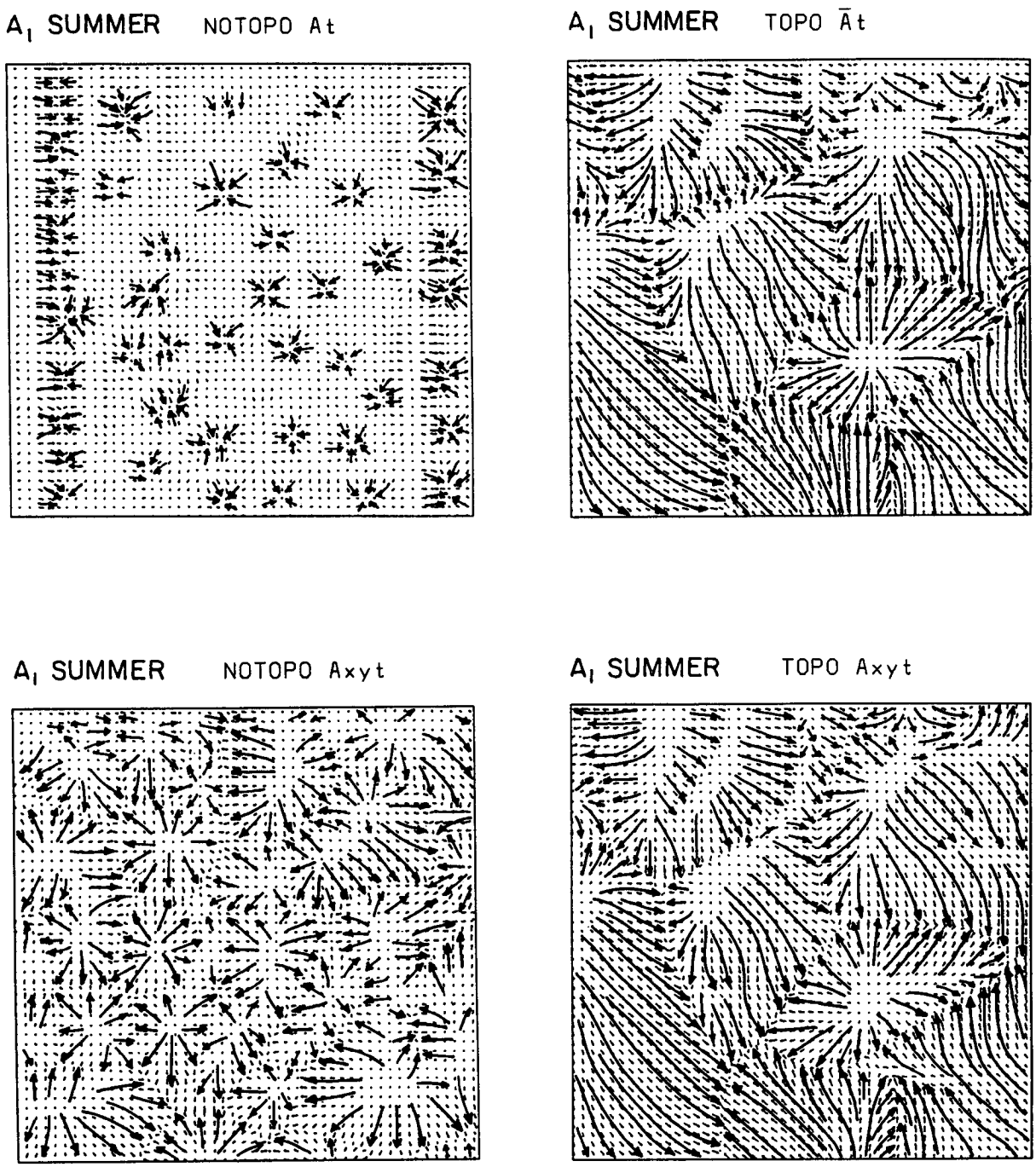

FIG. 8. Same as Figure 7 but for the summer simulation.

of 50 W m^{-2}, while the subgrid-scale fluxes at this level are 40–50 W m^{-2} also. During the summer, very substantial mesoscale and turbulent fluxes result from both the terrain and albedo variations.

The three-dimensional model results, constructed from observations of albedo derived from visible satellite images, suggest that albedo discontinuities can produce thermal mesoscale circulations with horizontal winds of around 5–10 m s^{-1}, the same magnitude as caused by terrain variability. However, with increasing synoptic winds, as discussed in Pielke et al. (1991), this effect would become less evident.

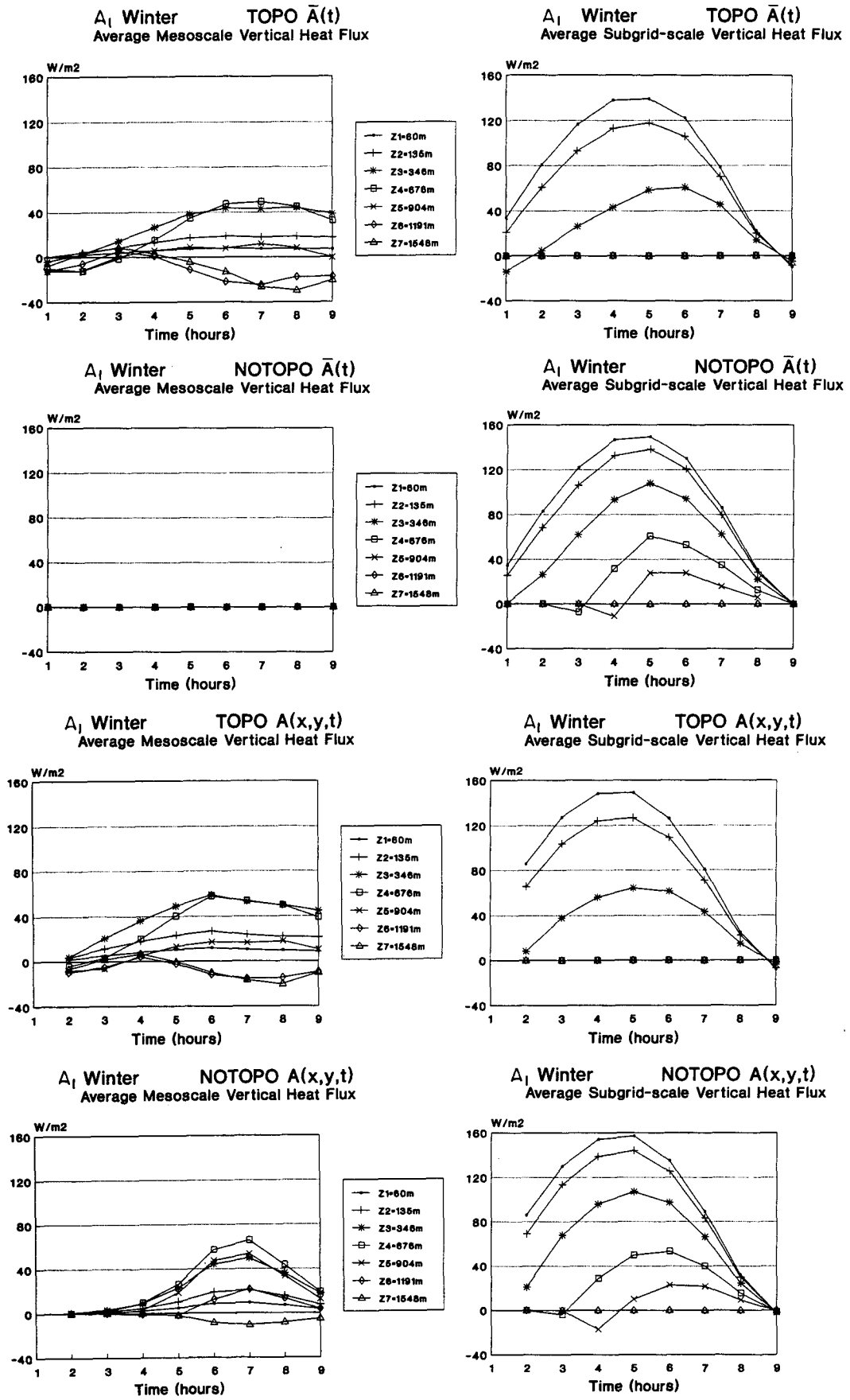

FIG. 9. Mesoscale and subgrid-scale heat fluxes at several levels for the winter case averaged across region A_1. Hour 1 corresponds to 0900 LST.

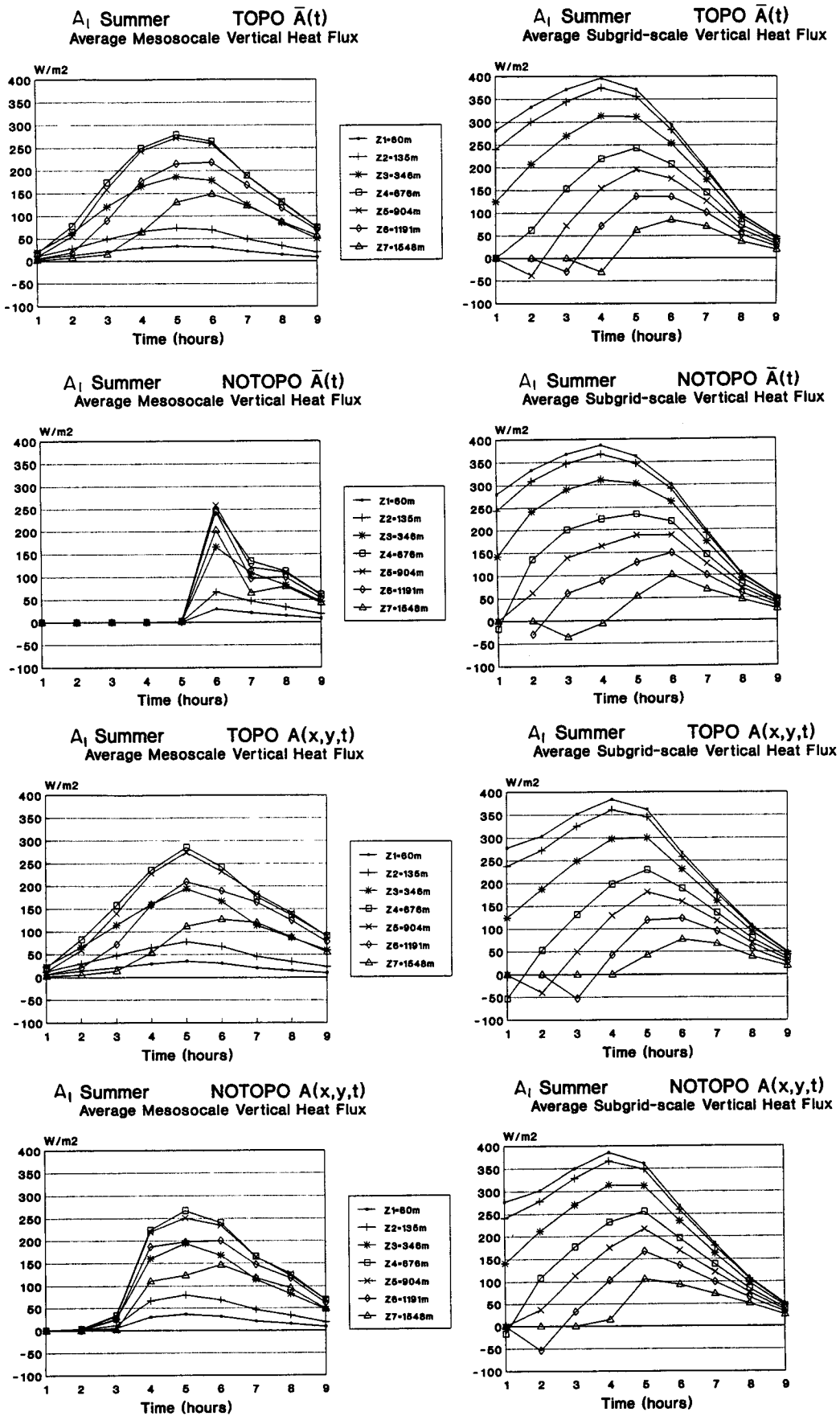

FIG. 10. Same as Fig. 9 but for the summer case.

3. Conclusions

This note demonstrates that mesoscale albedo variations are an important contribution to surface fluxes of heat and moisture, and to the development of thermally forced mesoscale circulations, particularly during the summer. As discussed in Pielke et al. (1991), the mesoscale fluxes generated by this spatial inhomogeneity must be considered in larger-scale models, including GCMs and numerical weather prediction models.

Acknowledgments. This work was supported under National Science Foundation Grant ATM-8915265 and funding was also provided by the National Park Service through Cooperative Agreement 1443-CA0001-92-006 to the Cooperative Institute for Research in the Atmosphere (Project 5-31796). Computer time was provided by the National Center for Atmospheric Research. NCAR is partially supported by the NSF. The satellite processing was completed by Kelly Dean. Dallas McDonald, Bryan Critchfield, and Tony Smith typed and edited the manuscript. One of the referees made several very effective comments on this paper, and the careful reading of the paper by that individual is appreciated.

REFERENCES

André, J.-C., P. Bougeault, J.-F. Mahfouf, P. Mascart, J. Noilhan, and J.-P. Pinty, 1989: Impact of forests on mesoscale meteorology. *Phil. Trans. Roy. Soc. Lond.*, **324**, 407–422.

Avissar, R., and R. A. Pielke, 1989: A parameterization of heterogeneous land surfaces for atmospheric numerical models and its impact on regional meteorology. *Mon. Wea. Rev.*, **117**, 2113–2136.

Chang, J., and P. J. Wetzel, 1991: Effects of spatial variations of soil moisture and vegetation on the evolution of a prestorm environment: A numerical case study. *Mon. Wea. Rev.*, **119**, 1368–1390.

Dalu, G. A., R. A. Pielke, R. Avissar, G. Kallos, M. Baldi, and A. Guerrini, 1991: Linear impact of thermal inhomogeneities on mesoscale atmospheric flow with zero synoptic wind. *Ann. Geophys.*, **9**, 641–647.

Klemp, J. B., and R. B. Wilhelmson, 1978a: The simulation of three-dimensional convective storm dynamics. *J. Atmos. Sci.*, **35**, 1070–1096.

——, and ——, 1978b: Simulations of right- and left-moving storms produced through storm splitting. *J. Atmos. Sci.*, **35**, 1097–1110.

Mahrer, Y., and R. A. Pielke, 1977: The effects of topography on sea and land breezes in a two-dimensional numerical model. *Mon. Wea. Rev.*, **105**, 1151–1162.

——, ——, 1978: The meteorological effect of the changes in surface albedo and moisture. *Israel Meteorological (IMS)*, Research Papers 2, 55–70.

Minnis, P., and E. F. Harrison, 1984: Diurnal variability of regional cloud and clear-sky radiative parameters derived from GOES data. Part I: Analysis method. *J. Climate and Appl. Meteor.*, **23**, 993–1011.

Otterman, J., 1977: Anthropogenic impact on the albedo of the earth. *Clim. Change*, **1**, 137–155.

Pielke, R. A., 1984: *Mesoscale Meteorological Modeling.* Academic Press, 612 pp.

——, and X. Zeng, 1989: Influence on severe storm development of irrigated land. *Natl. Wea. Dig.*, **14**, 16–17.

——, G. Dalu, J. S. Snook, T. J. Lee, and T. G. F. Kittel, 1991: Nonlinear influence of mesoscale land use on weather and climate. *J. Climate*, **4**, 1053–1069.

——, W. R. Cotton, R. L. Walko, C. J. Tremback, M. E. Nicholls, M. D. Moran, D. A. Wesley, T. J. Lee, and J. H. Copeland, 1992: A comprehensive meteorological modeling system—RAMS. *Meteor. Atmos. Phys.*, **49**, 69–91.

Segal, M., R. Avissar, M. C. McCumber, and R. A. Pielke, 1988: Evaluation of vegetation effects on the generation and modification of mesoscale circulations. *J. Atmos. Sci.*, **45**, 2268–2292.

——, W. Schreiber, G. Kallos, R. A. Pielke, J. R. Garratt, J. Weaver, A. Rodi, and J. Wilson, 1989: The impact of crop areas in northeast Colorado on midsummer mesoscale thermal circulations. *Mon. Wea. Rev.*, **117**, 809–825.

Tremback, C. J., and R. Kessler, 1985: A surface temperature and moisture parameterization for use in mesoscale numerical models. Preprints, *7th Conf. on Numerical Weather Prediction*, Montreal, Canada, Amer. Meteor. Soc.